Chapter 3

Solution Structure and Behavior of Palladium Allyl Carboxylates and Carbonates †

3.1 Introduction

By monitoring the palladium-catalyzed decarboxylative allylic alkylation of allyl β-ketoester **7**, palladium carboxylate **31** was discovered and subsequently isolated (Scheme 3.1 on page 132).[1] Carboxylate **31** was identified as a significant intermediate in this reaction and determined to be the resting state of the active catalyst.[1] Carboxylate **31** and its subsequently synthesized parent **32** represent a series of unusual palladium η^1-allyl carboxylate complexes with previously unstudied properties (Figure 3.1 on page 132). Beyond the actual role of carboxylate **31** in the allylic alkylation reaction, carboxylates **31** and **32** are thought to represent the best isolable model systems currently available for the elusive and important intermediate, palladium enolate **27**.[2,3] Carboxylates **31** and **32** may also represent potentially significant model systems for the study of other palladium-catalyzed reactions, such as allylic oxidation[4,5] and 1,4-diacetoxylation.[4,6] As a result, the nature of the solution structures and dynamic behavior

† This work was done in collaboration with Dr. David VanderVelde.

of palladium allyl carboxylates **31** and **32** are potentially relevant to the mechanistic understanding of a number of different palladium-catalyzed reactions. To this effect, a thorough study of the solution structure and chemical behavior of isolated samples of carboxylates **31** and **32** was undertaken.

*Scheme 3.1. Initial Observation of Palladium Allyl Carboxylate **31***

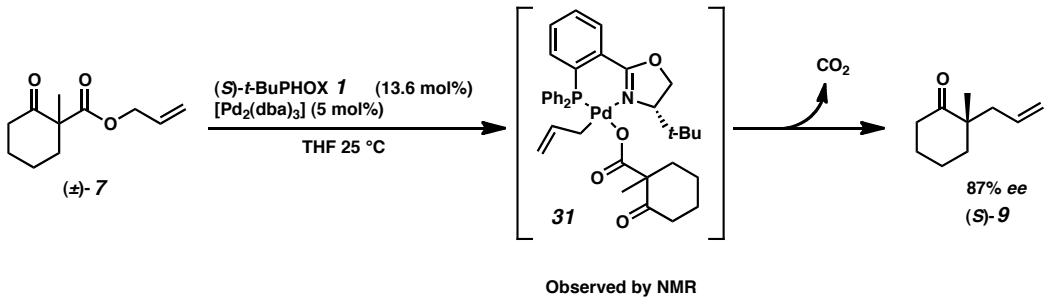

Figure 3.1. Palladium η^1 Allyl Species of Interest to the Study of Allylic Alkylation

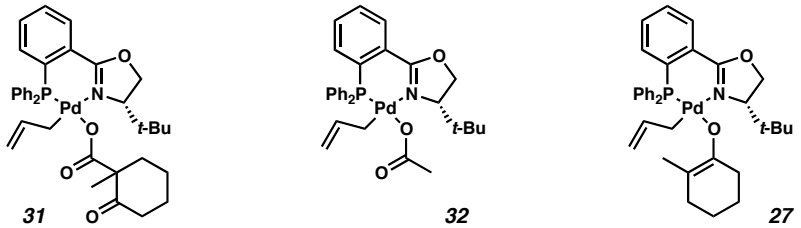

3.2 **Analyzing Solution Structure and Chemical Behavior via NMR**

*3.2.1 The Solution Structure of Carboxylates **31** and **32***

Examining complexes **31** and **32** by 1D and 2D NMR methods revealed that even at –20 °C these species possess a significant amount of dynamic chemical behavior when dissolved in $THF_{d\text{-}8}$. It is clear by NMR that the structures found in the solid state for complexes **31** and **32**, consisting of an η^1-allyl ligand *cis* to an associated carboxylate ligand, is the dominant structure found for these species in solution as well. While 2D

^{1}H-^{1}H NOESY and ROESY spectra helped confirm these solution structures,[7] the strongest indication of the allyl ligand hapticity actually came from the 1D ^{1}H and ^{13}C NMR chemical shifts for the allyl ligands (Figure 3.2 on page 133 and Figure 3.3 on page 134). The resonances found for the allyl ligand in complexes **31** and **32** are consistent with those of other fully characterized and highly related palladium η^1-allyl complexes reported in the literature.[8,9]

The 1D ^{13}C NMR spectrum was the most sensitive tool for distinguishing between the η^1 and η^3 allyl ligands. While still noticeably shifted, the ^{13}C NMR chemical shifts for the allyl ligands of complexes **31** and **32** are closer to those found in free propene when dissolved in $THF_{d\text{-}8}$ then they are to those found in the corresponding π-allyl cation **25** (Figure 3.2).[10] The increased delocalization of the π-allyl ligand in **25** causes the chemical shifts for the protons and carbons found in the allyl ligand to shift inwards towards one another relative to the same resonances found in the complexes with η^1-allyl ligands. This chemical shift averaging effect for the atoms in the allyl ligand of cation **25** is also manifested more strongly in the carbon spectrum then it is in the proton (Figure 3.2).

*Figure 3.2. Characteristic η^1 and η^3 Allyl ^{13}C NMR Shifts (δ) Found for **31**, **32**, and **25** in $THF_{d\text{-}8}$*

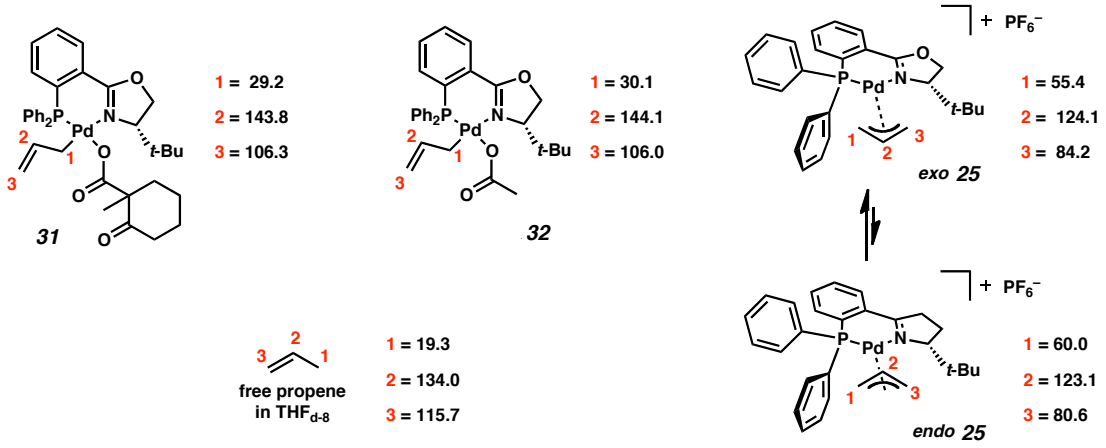

*Figure 3.3. Characteristic η^1 and η^3 Allyl ^{1}H NMR Shifts (δ) Found for **31**, **32**, and **25** in $THF_{d\text{-}8}$*

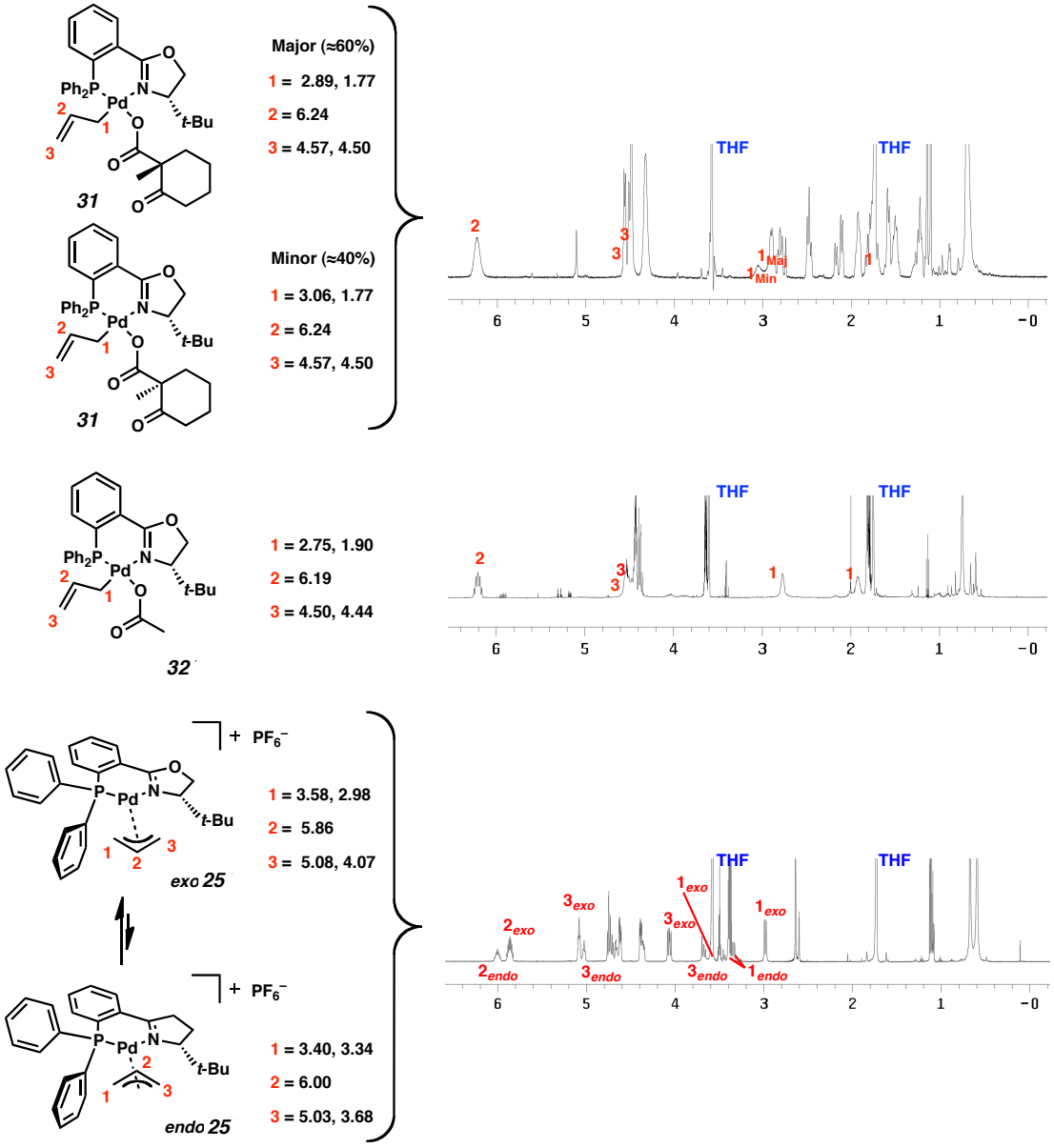

^{1}H NMR spectra of complexes **31**, **32**, and **25** in $THF_{d\text{-}8}$. The spectra were taken at –20°C for the stability of complex **31** which is prone to thermal decomposition near room temperature. Temperature was the same across all three spectra for the sake of comparison. The region highlighted, is δ = 6.8 to –0.2 ppm.

*3.2.2 The Chemical Behavior of Carboxylates **31** and **32** in Solution*

Much of the dynamic chemical behavior of complexes **31** and **32** in THF solution occurring on the NMR time scale can be observed directly as chemical exchange in the

corresponding 2D EXSY NMR spectrum.[11] The exchange patterns found for both complexes **31** and **32** indicate complete allyl termini exchange (Figure 3.4 on page 135).[12] EXSY cross peaks show that the two vinyl termini protons ($3_\alpha \leftrightarrow 3_\beta$) and the two alkyl protons ($1_\alpha \leftrightarrow 1_\beta$) of the allyl ligands in carboxylates **31** and **32** rapidly interconvert with one another on the NMR timescale even at temperatures as low as –20°C in $THF_{d\text{-}8}$. While implied, the cross-peaks indicating interconversion of the two protons at each termini between one another (i.e., $1_\alpha \leftrightarrow 1_\beta$ and $3_\alpha \leftrightarrow 3_\beta$) for complexes **31** and **32** do not show up well in the EXSY spectra. This is because the corresponding EXSY cross-peaks are eclipsed by strong through space NOESY and ROESY cross-peaks of the opposite phase.[13]

*Figure 3.4. Allyl Termini Exchange Patterns for **31** and **32**[12]*

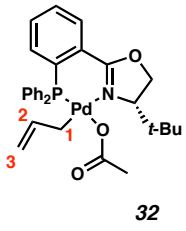

32

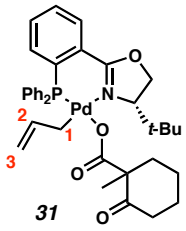

31

Exchange Table

	1_α	1_β	2	3_α	3_β
1_α		w		s	s
1_β	w			s	s
2					
3_α	s	s			i
3_β	s	s		i	

Exchange Table

	1_α (maj)	1_α (min)	1_β	2	3_α	3_β
1_α (maj)		s	i		s	s
1_α (min)	s		i		s	s
1_β	i	i			s	s
2						
3_α	s	s	s			i
3_β	s	s	s		i	

Exchange tables showing which protons exchange with each other on an NMR timescale in $THF_{d\text{-}8}$ for **32** at 0°C and for **31** –20°C[12]

The exchange patterns documented in Figure 3.4 indirectly imply a more elaborate pattern of chemical behavior for complexes **31** and **32**, as rapid allyl termini

exchange is generally not observed for stable palladium η^1-allyl complexes directly.[8c,14] Complete allyl termini exchange is, however, highly consistent with the reported solution behavior for a large number of palladium π-allyl complexes.[15] Indeed evidence of significant, but transient, η^3-allyl behavior is observed by NMR for both complexes **31** and **32** in solution. One of the most compelling indications of this is found in the EXSY NMR exchange between the diastereotopic alkyl methylene protons between the two diastereomers of palladium allyl carboxylate **31** (i.e., $1_{\alpha\text{-maj}} \leftrightarrow 1_{\alpha\text{-min}}$ in the exchange table for **31** in Figure 3.4 on page 135).

There are only three theoretical mechanisms that can explain chemical exchange between the two diastereomers of **31**: rapid racemization of the PHOX ligand, rapid racemization of the all-carbon quaternary stereocenter on the carboxylate ligand, or rapid exchange of the carboxylate ligands between palladium allyl species (Scheme 3.2 on page 137).[16] Rapid racemization of the PHOX ligand in THF cannot be possible or else the enantioenriched allylic alkylation product, ketone **9** (Scheme 3.1 on page 132), produced by carboxylate **31** would be would be formed almost racemically under reaction conditions. Rapid racemization of the carboxylate all-carbon quaternary stereocenter is not possible as the stereochemical purity of this quaternary center is actually modestly amplified when synthesizing carboxylate **31** from racemic allyl β-ketoester **7** (Scheme 3.3 on page 137).[17] Similarly, ^{1}H NMR shows that the d.r. for isolated samples of **31** does not change over time in solution, disproving the hypothetical epimerization processes of the quaternary center. However, the rapid exchange of potentially labile anionic ligands, such as a carboxylate, between palladium(II) allyl species, is both feasible and well precedented.[18]

*Scheme 3.2. The Three Possible Mechanisms for Chemical Exchange Between (*R,S) and (*S,S*) ***31***

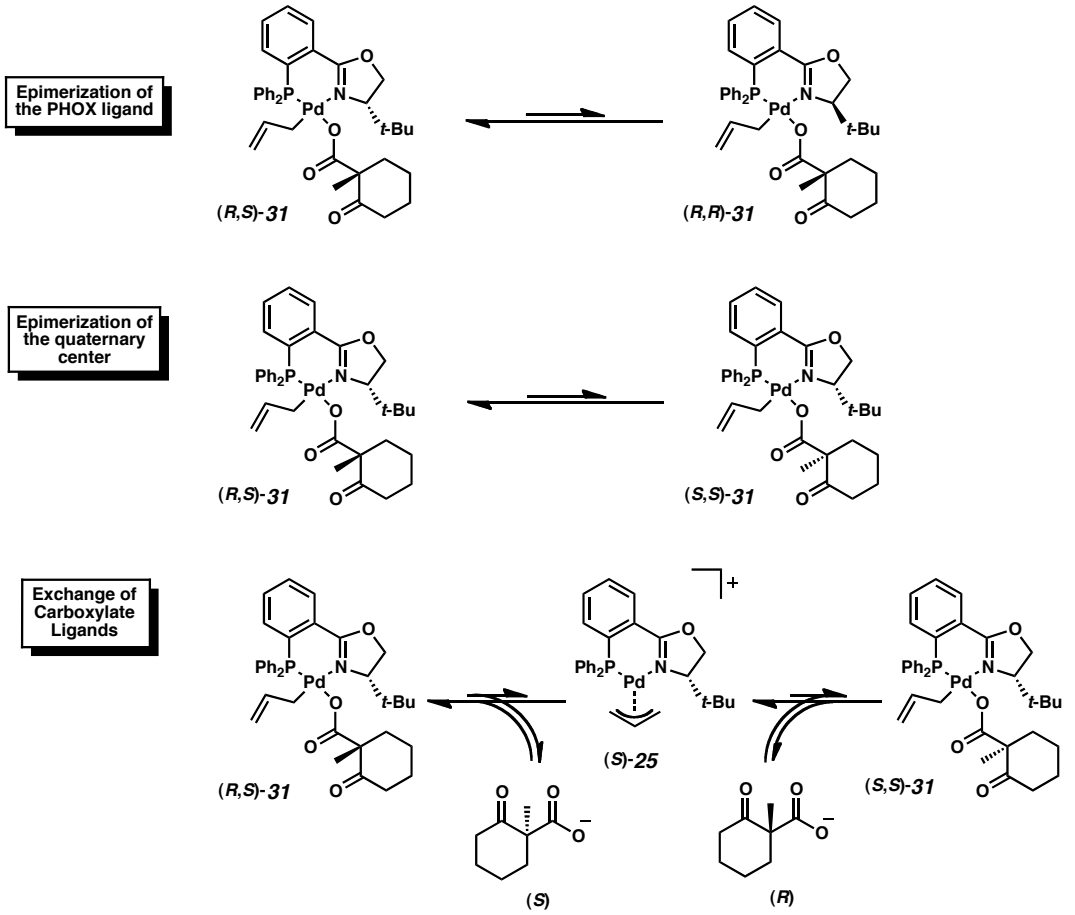

Scheme 3.3. Stereochemical Enrichment of The Quaternary Center in the Synthesis of ***31***

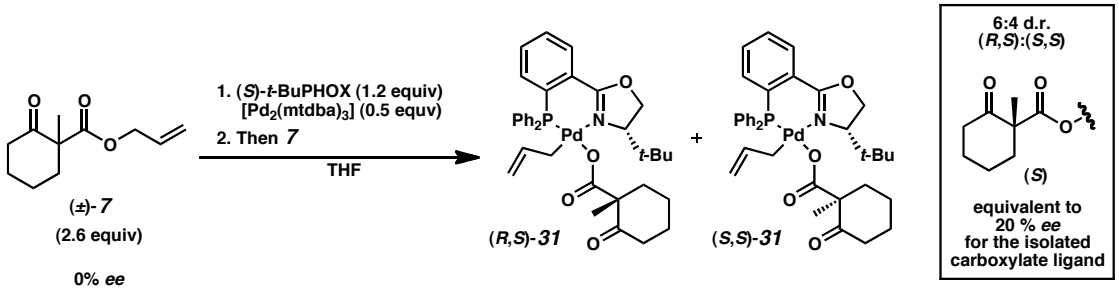

Thus, the observed diastereotopic chemical exchange cross-peak for carboxylate **31** is indicative of a particularly rapid exchange of carboxylate ligands between individual molecules of **31**. Given the high degree of similarity between complexes **31** and **32**, it is expected that acetate ligands exchange rapidly between molecules of **32**

when in solution. However, the lack of diastereomers in carboxylate **32** eliminates the possibility of EXSY cross-peaks that could indicate this exchange.

In the absence of a carboxylate or other coordinating ligand, complexes **31** and **32** have a preferred η^3-allyl structure as demonstrated by their corresponding π-allyl cation **25**. Complexes **31** and **32** should therefore be in equilibrium with π-allyl cation **25** at least transiently while carboxylate ligands are being exchanged between the molecules of these complexes.[19] As π-allyl cation **25** is in equilibrium with carboxylates **31** and **32**, it would be reasonable to consider that **25** might be the source of the complete allyl termini scrambling observed for carboxylates **31** and **32**.

3.3 Analyzing the Solution Behavior of π-Allyl Cation 25 by NMR

*3.3.1 EXSY Spectra for π-Allyl Cation **25***

Surprisingly, the 2D NMR EXSY spectrum of palladium π-allyl cation **25** exhibits a far simpler pattern of chemical exchange then either complex **31** or **32** (Figure 3.5 on page 139). The EXSY spectrum of palladium π-allyl cation **25** is consistent with only a single exchange pathway between its *endo* and *exo* isomers through a simple η^3-η^1-η^3 allyl isomerization. While two such isomerization paths are possible, only the η^3-η^1-η^3 allyl isomerization event where the η^1-allyl intermediate is *trans* to the sp^2 nitrogen is observed for π-allyl cation **25** (Figure 3.6 on page 139).[20] Significantly this corresponds to the same regioselective *trans*-N η^1-allyl isomer as seen in carboxylate complexes **31** and **32**. While most palladium π-allyl complexes exhibit a more intricate suite of allyl isomerization modes,[23] related palladium PHOX complexes,[20] as well as

other more distant ligand frameworks,[21] have also given rise to palladium π-allyl complexes that exhibit only a single regioselective η^3-η^1-η^3 allyl isomerization mode as is observed for complex **25**.

Figure 3.5. Allyl Exchange Pattern Between Endo *and* Exo ***25***[12]

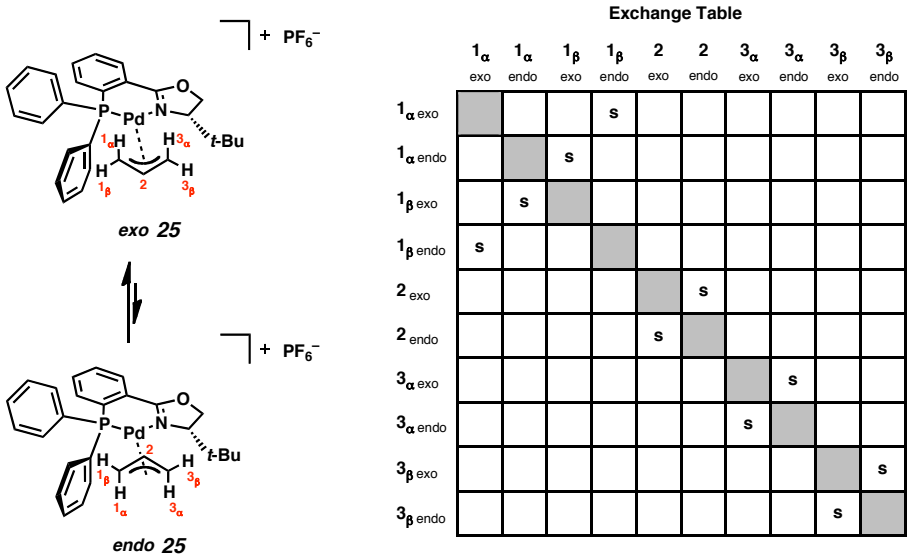

Exchange table showing which protons exchange on an NMR timescale in $THF_{d\text{-}8}$ for **25**. The depicted exchange pattern is constant from –25 °C up to where complex **25** approaches coalescence at 60 °C.[12]

Figure 3.6. The Only Allyl Isomerization Mode Observable for ***25***.

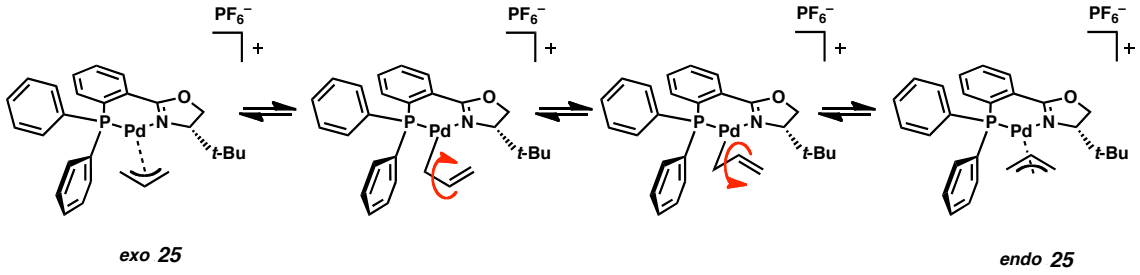

3.3.2 Analyzing the Exo/Endo *Isomerization Mechanism of* ***25***

Saturation transfer NMR techniques were used to obtain the kinetics data for the allyl isomerization of **25** in $THF_{d\text{-}8}$ and an Eyring plot was constructed. The activation

parameters thus determined show a negative entropy of activation (Figure 3.8 on page 141).[12] Similarly while the ^{1}H NMR spectra of **25** is sharp and well resolved at 25 °C in $CDCl_3$, the same spectra in the less polar but more strongly coordinating solvent $THF_{d\text{-}8}$ is poorly resolved (Figure 3.7 on page 140). This is a result of allyl isomerization accelerating from slow exchange, observed in $CDCl_3$ at 25 °C, to a point approaching intermediate exchange, observed in $THF_{d\text{-}8}$ at 25 °C. Cooling solutions of **25** in $THF_{d\text{-}8}$ down to –5 °C or below produces sharp, well-resolved resonances like those seen in $CDCl_3$ at 25 °C. This is indicative of the allyl isomerization being accelerated by THF, and then approaching the slower rate of isomerization found in $CDCl_3$ when the THF solution is cooled.

Figure 3.7. ^{1}H NMR Broadening Indicating $THF_{d\text{-}8}$ Accelerated Allyl Isomerization Relative to $CDCl_3$

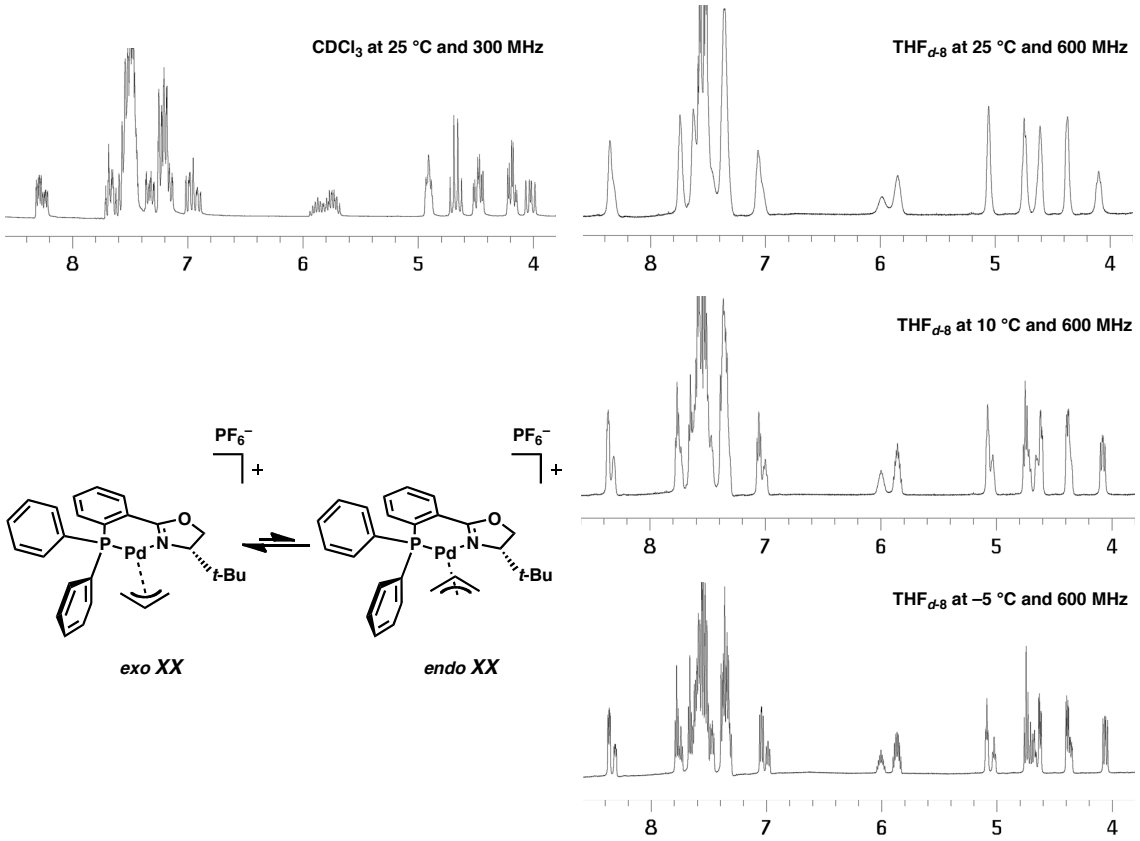

The addition of 4.4 equivalents of water, a modest but slightly superior nucleophile relative to THF, more then doubled the rate of the allyl isomerization as measured by saturation transfer (Figure 3.8 on page 141). Altogether, this data indicates that the η^3-η^1-η^3 allyl isomerization mode for palladium π-allyl cation **25** functions via an associative mechanism. By this mechanism, nucleophiles, such as THF, water, and carboxylate anions, can associate with π-allyl complex **25** and facilitate a *trans*-N regioselective η^3-η^1-η^3 allyl isomerization with bond rotation (Figure 3.9 on page 142 and Figure 3.10 on page 142).[22] Similar associative η^3-η^1-η^3 allyl isomerization mechanisms have been reported for other palladium π-allyl complexes.[18b] Ironically, this means that the mechanism for the only observed allyl isomerization mode active in π-allyl complex **25** between –25 and 60 °C requires species like carboxylates **31** and **32** as intermediates.

Figure 3.8. Activation Parameters for Exo/Endo *Allyl Isomerization of* ***25***

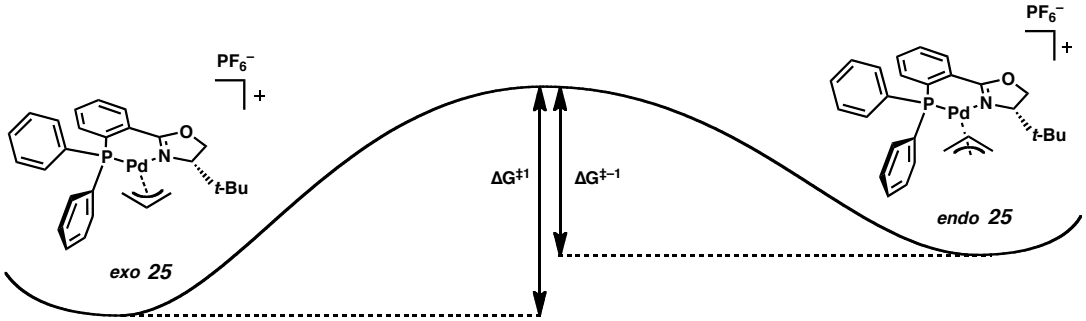

	$\Delta G^{\ddagger 1}$	$\Delta G^{\ddagger -1}$
$THF_{d\text{-}8}$ with 3 mol% water:	$\Delta H^{\ddagger}$ = 8.0 kcal/mol $\Delta S^{\ddagger}$ = –27 cal/mol·K	$\Delta H^{\ddagger}$ = 8.3 kcal/mol $\Delta S^{\ddagger}$ = –25 cal/mol·K
$THF_{d\text{-}8}$ with 4.4 equiv water:	$\Delta H^{\ddagger}$ = 7.7 kcal/mol $\Delta S^{\ddagger}$ = –26 cal/mol·K	$\Delta H^{\ddagger}$ = 7.9 kcal/mol $\Delta S^{\ddagger}$ = –24 cal/mol·K

Table 3.1. Some Select Rates and the Effects of Water on the Exo/Endo *Allyl Isomerization of* ***25***

	exo → endo	***endo → exo***
3.04 mol% water:	**5°C = 4.49 s^{-1}** **–5°C = 2.36 s^{-1}** **–10°C = 1.80 s^{-1}**	**5°C = 7.40 s^{-1}** **–5°C = 3.88 s^{-1}** **–10°C = 2.88 s^{-1}**
4.4 equiv water:	**5°C = 9.56 s^{-1}** **–5°C = 5.83 s^{-1}** **–10°C = 4.08 s^{-1}**	**5°C = 15.86 s^{-1}** **–5°C = 13.53 s^{-1}** **–10°C = 7.31 s^{-1}**

Figure 3.9. Equatorial Associative Exo/Endo *Allyl Isomerization Mechanism of* ***25*** *as Demonstrated for Carboxylate Nucleophiles by Complexes* ***31*** *and* ***32***[22]

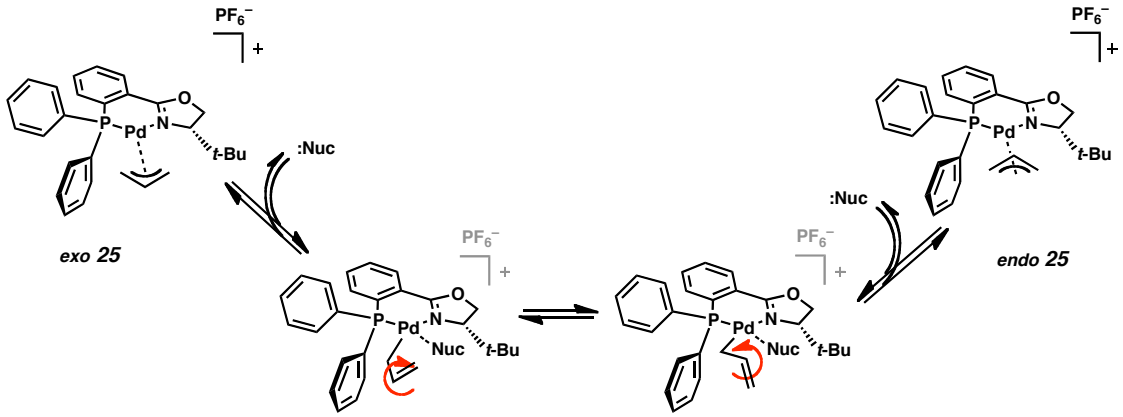

Figure 3.10. Possible Apical Associative Exo/Endo *Allyl Isomerization Mechanism of* ***25***[22]

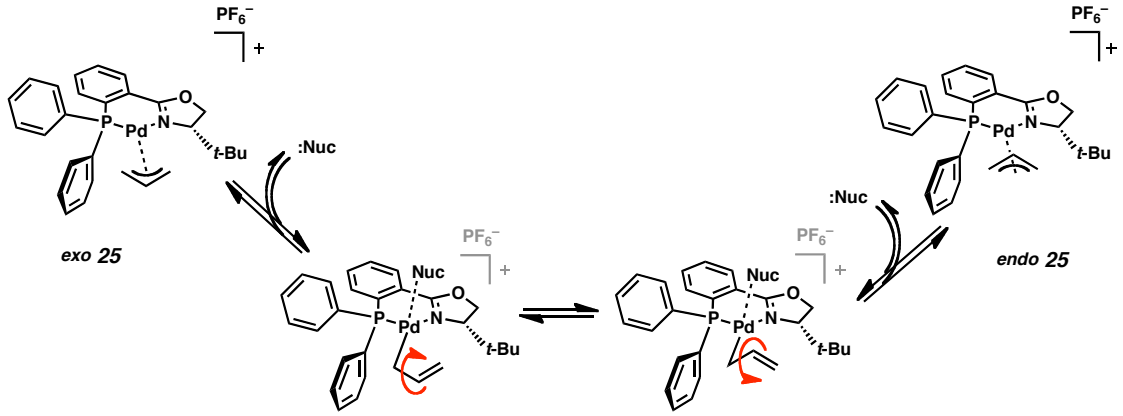

3.3.3 No Allyl Termini Scrambling Caused by π-Allyl Cation ***25***

The simple regioselective η^3-η^1-η^3 allyl isomerization pathway demonstrated by palladium π-allyl cation **25** cannot interchange all of the allyl termini protons. For the complete allyl termini exchange seen in carboxylate complexes **31** and **32** to be a result

of allyl isomerization from π-allyl cation **25**, other common allyl isomerization modes would be necessary. At a bare minimum, π-allyl cation **25** would need an apparent allyl rotation isomerization mode in addition to the observed regioselective *exo*/*endo* exchange path to be able to completely exchange all the protons in the allyl ligand termini (Figure 3.11 on page 143).[23]

*Figure 3.11. Minimum Isomerization Modes Necessary for **25** to Facilitate Complete Allyl Termini Exchange as Observed for Carboxylates **31** and **32***

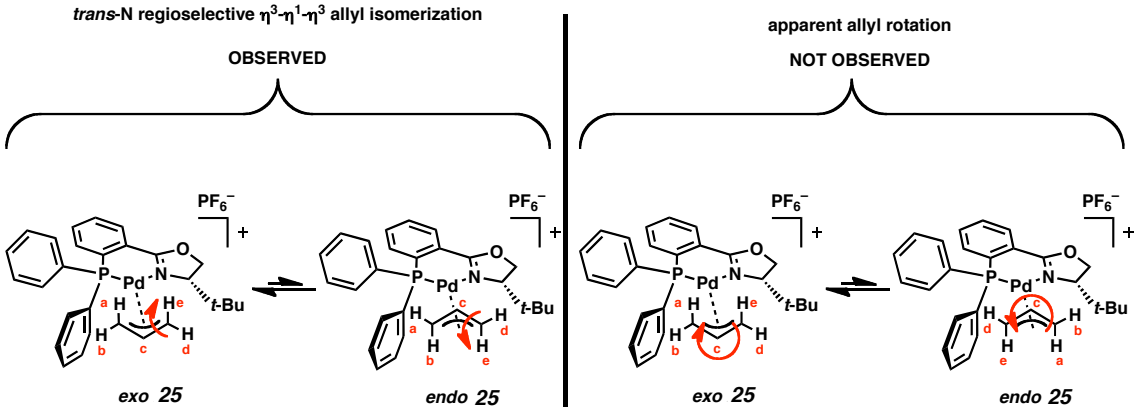

To this effect, additional isomerization modes were sought for π-allyl cation **25** at higher temperatures. Examining both the ^{1}H and EXSY NMR spectra for π-allyl cation **25** in $THF_{d\text{-}8}$ taken at 60 °C showed the simple regioselective *trans*-N η^3-η^1-η^3 isomerization mode approaching complete coalescence. However, no new allyl isomerization pathways could be observed for π-allyl cation **25** in the EXSY spectrum. This eliminates the possibility that other allyl isomerization modes, possibly accelerated by the presence of carboxylate anions, could be active for π-allyl cation **25** at –25 °C but too slow to be observed by NMR at that temperature. As a result, the complete allyl termini exchange of carboxylate complexes **31** and **32** cannot be explained via the chemical behavior of the corresponding π-allyl cation **25** with which they are in

equilibrium. The allyl termini scrambling observed in carboxylates **31** and **32** must instead be the result of a mechanism that does not directly involve π-allyl cation **25**.

3.4 Allyl Termini Scrambling via Oxidative Addition and Reductive Elimination

3.4.1 The Oxidative Addition and Reductive Elimination Equilibrium

The chemical process that gives a more satisfying explanation for the rapid and complete allyl termini exchange found in carboxylate complexes **31** and **32** is reductive elimination and oxidative addition. While little direct evidence of such an equilibrium can be observed for carboxylate complex **31**, the equivalent equilibrium is clearly visible in solution for the parent allyl acetate complex **32**. All samples of allyl acetate complex **32**, despite being verified as pure in the solid state by both elemental analysis and X-ray crystallography, show traces of other species in solution by NMR (Figure 3.12 on page 146). Of note, NMR integration shows that these minor species have a constant ratio of composition across different batches of **32**. This suggests that these species are part of an equilibrium involving carboxylate **32**.

The majority of these minor complexes are too weak to be fully analyzed by most spectrographic means (approximately less then 1% composition in solution) making them difficult to analyze. However, there is a second complete set of resonances representing about 4% of the mass balance based on integration in both the ^{1}H and ^{31}P NMR (circled resonances in the middle and top spectra in Figure 3.12). This second set of 4% intensity resonances corresponds to free allyl acetate,[10] and what is believed to be either [{(*S*)-*t*-BuPHOX}Pd(0)] or its corresponding solvento complex (allyl acetate resonances circled

in blue in the middle spectrum and compared to free allyl acetate in the bottom spectrum, [{(*S*)-*t*-BuPHOX}Pd(0)] resonances circled in red in the top and middle spectra in Figure 3.12). This suggests that carboxylate complex **32** is part of a rapid equilibrium involving the reductive elimination and oxidative addition of allyl acetate (Scheme 3.4 on page 145). By analogy, carboxylate complex **31** is believed to be involved in a similar equilibrium (Scheme 3.5 on page 145). Related equilibria between palladium π-allyl cations with carboxylate counter ions and the corresponding allylic esters are well precedented in the literature (Scheme 3.6 on page 145).[24]

*Scheme 3.4. Allyl Acetate Reductive Elimination and Oxidative Addition Observed for **32** in $THF_{d\text{-}8}$*

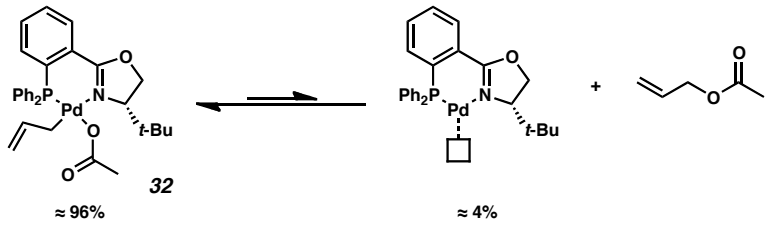

*Scheme 3.5. Implied Equilibrium for Carboxylate **31** by Analogy to **32***

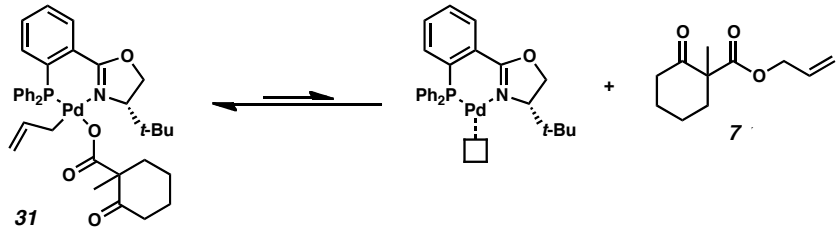

Scheme 3.6. Select Examples of Previously Reported Systems with Palladium Allyl Species in Equilibrium with Allyl Carboxylates[24a,b]

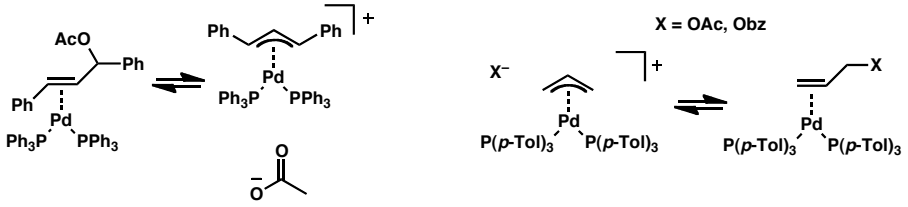

Figure 3.12. Apparent Free Allyl Acetate and Second Palladium Species in Equilibrium with ***32***

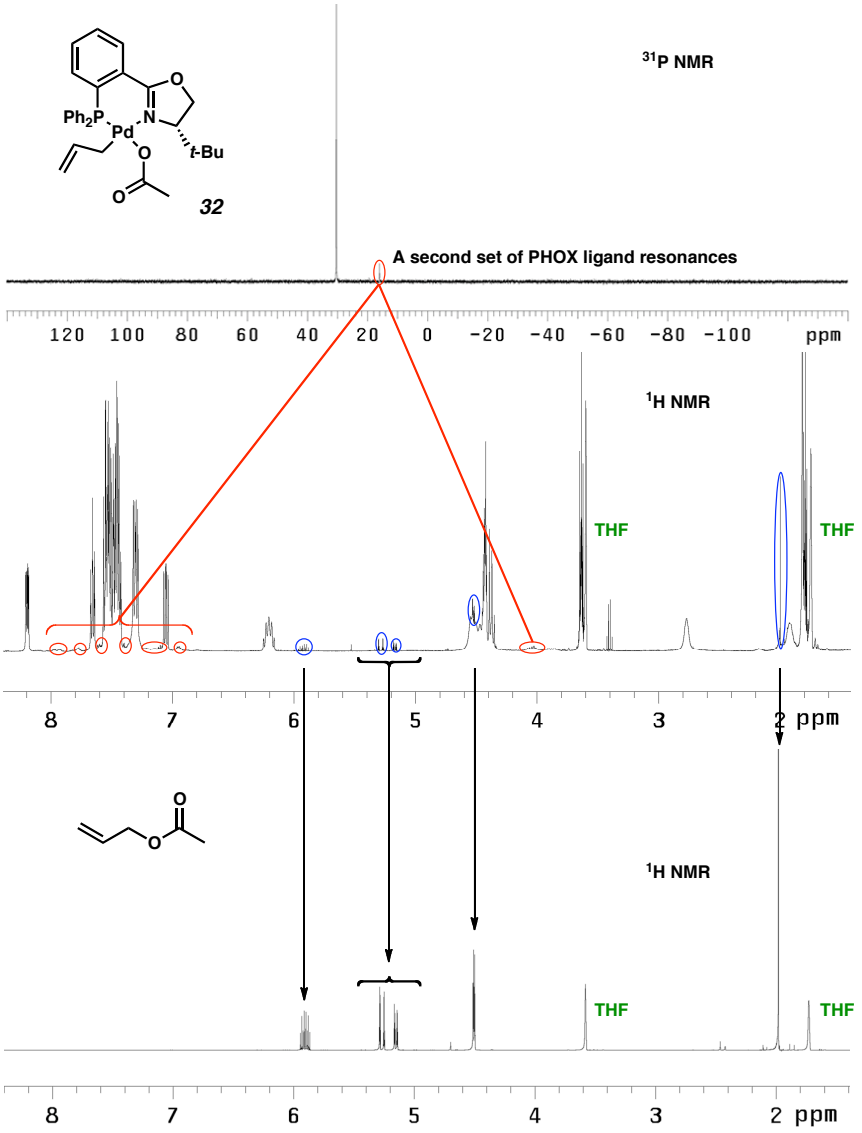

Top spectrum: ^{31}P NMR in $THF_{d\text{-}8}$ of a pure sample of complex **32** reveals a second minor phosphorous resonance upfield of the resonance associated with complex **32**. This minor resonance corresponds to about 4% of the total phosphorus integration. Middle spectrum: ^{1}H NMR in $THF_{d\text{-}8}$ of the same sample of complex **32** shows a second set of PHOX ligand proton resonances. These resonances integrate 4:96 against the corresponding PHOX ligand resonances associated with **32**. The middle spectrum also shows a set of resonances that appear to correspond to free allyl acetate. Bottom spectrum: ^{1}H NMR in $THF_{d\text{-}8}$ of free allyl acetate showing a perfect match to the allyl acetate resonances found in the middle spectrum.

3.4.2 Possible Mechanisms for Allyl Termini Scrambling

The equilibrium for complexes **31** and **32** consisting of facile reductive elimination and oxidative addition of allyl carboxylates, can easily account for the rapid and complete allyl termini scrambling observed for these complexes. There are four general mechanisms by which this scrambling could be possible via this equilibrium. Both reductive elimination and oxidative addition could be only weakly or even non-regioselective (top scenario pictured in Figure 3.13 on page 148). Either reductive elimination, or oxidative addition could be only weakly or even non-regioselective while its reverse is selective (middle four scenarios pictured in Figure 3.13). Oxidative addition and reductive elimination could both be regioselective but with strong preferences towards opposite termini of the allyl group from one another (bottom two scenarios pictured in Figure 3.13).

Figure 3.13. Possible Means of Allyl Termini Scrambling via the Allyl Carboxylate Equilibrium

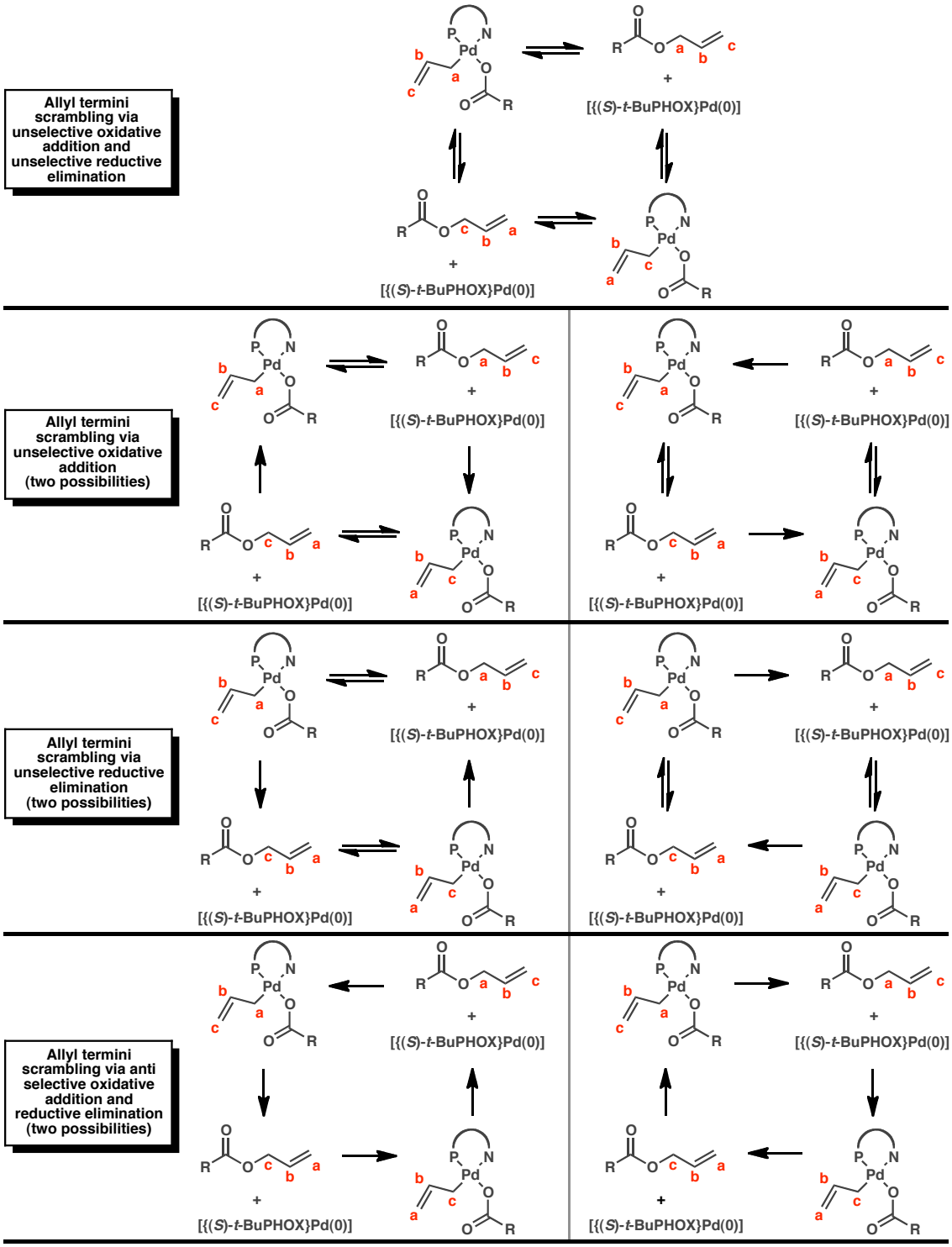

3.5 Examining Selectivity in Reductive Elimination

3.5.1 Literature Precedent For the Reductive Elimination of Allyl Carboxylates

While the possibilities presented in Figure 3.13 (page 148) cannot be narrowed down farther with the current data alone, the literature on related studies recommends only two of the possibilities depicted in Figure 3.13. Much is already understood about the reductive elimination of allylic acetates from palladium(II) centers due to investigation of processes like palladium-catalyzed allylic oxidation and 1,4-diacetoxylation.[4,5,6] Two competing paths have been reported for the reductive elimination of allylic acetates from palladium species. The first pathway is an outer-sphere attack of an acetate anion on an η^3-allyl terminus (Figure 3.14 left, on page 150). This mechanism is simply an instance of palladium-catalyzed outer-sphere allylic alkylation of carbon nucleophiles.[2,4,5,6] The second pathway is an internal *cis* migration of the carboxylate ligand (Figure 3.14 right). This mechanism is synonymous with palladium-catalyzed inner-sphere allylic alkylation via doubly vinylogous reductive elimination. [2,3,4,5,6] Thus, the formation of allylic acetates via reductive elimination from palladium(II) allyl acetate species is effectively a specific subset of the well-studied general field of palladium-catalyzed allylic alkylation. Mechanistically this suggests that the reductive elimination of allylic carboxylates from palladium is heavily parallel to the mechanism of palladium-catalyzed allylic alkylation of α-β unsaturated carbon nucleophiles (e.g., ketone enolates).

Figure 3.14. Reported Mechanisms for Palladium Allyl Carboxylate Reductive Elimination[4,5,6]

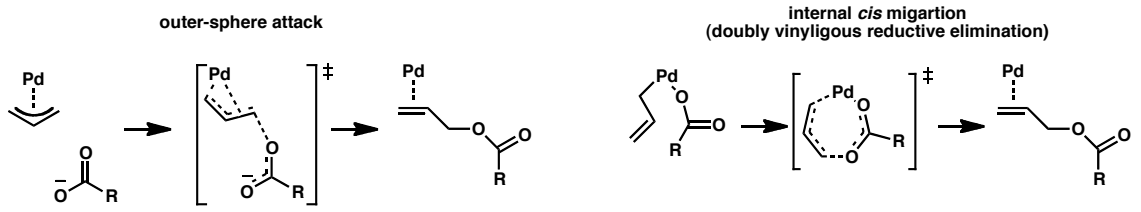

3.5.2 Mechanistic Possibilities with Selective Reductive Elimination

The studies of palladium-catalyzed allylic oxidation suggest that the reductive elimination of allyl acetates from palladium complexes possessing η^1-allyl ligands *cis* to associated acetate ligands generally prefer to proceed via the inner-sphere doubly vinylogous reductive elimination pathway (Figure 3.14 left on page 150).[4,5,6] However, the preference between the two mechanisms depicted in Figure 3.14 is expected to be irrelevant for allyl terminus selectivity in reductive elimination from carboxylates **31** and **32**. This is because the literature precedent for both outer-sphere and inner-sphere allylic alkylation with PHOX palladium allyl species universally states that both mechanisms are regiospecific to the allyl terminus *trans* to phosphorous (Scheme 3.7 on page 151).[2,3,25] As a result, regardless of which mechanistic path is preferred or what distribution of both paths may be taken, reductive elimination of allylic carboxylates from complexes **31** and **32** is postulated to have a very high allyl terminus regioselectivity (*trans*-P).

Scheme 3.7. The Same Allyl Terminus Selectivity is Expected for the Two Standard Mechanisms of Allyl Carboxylate Reductive Elimination in PHOX Palladium Allyl Carboxylates.

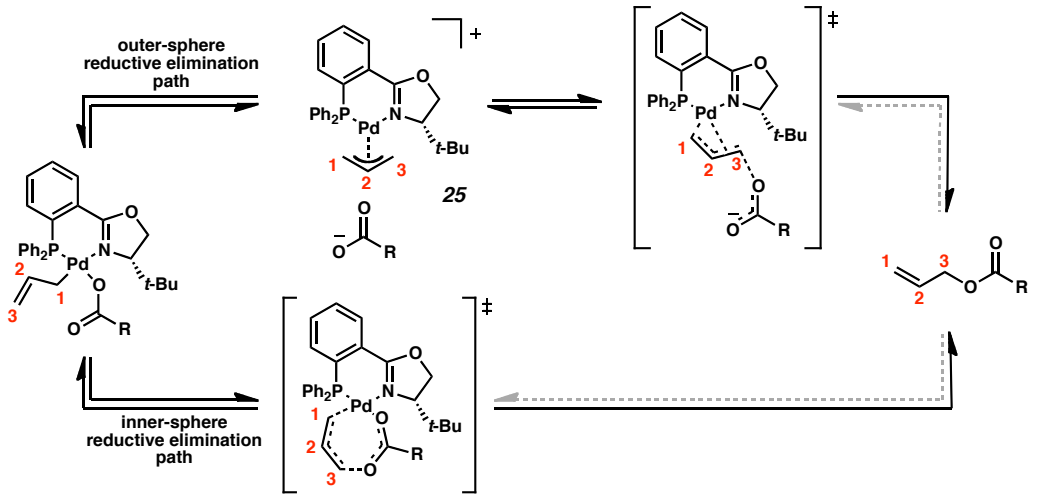

This would suggest that allyl termini scrambling in this system may actually be a result of oxidative addition. If correct, either oxidative addition of allylic carboxylates is non-selective, or it is anti-selective relative to the reductive elimination pathways (Figure 3.15 on page 151).[26] While farther experimentation is necessary to examine the possibility of this mechanistic hypothesis, the two mechanisms for allyl termini scrambling in Figure 3.15 are those most strongly consistent with both the acquired data and the accepted chemical behavior found in the litterature.[2,3,25]

Figure 3.15. Allyl Termini Scrambling Mechanisms Most Consistent with the Literature

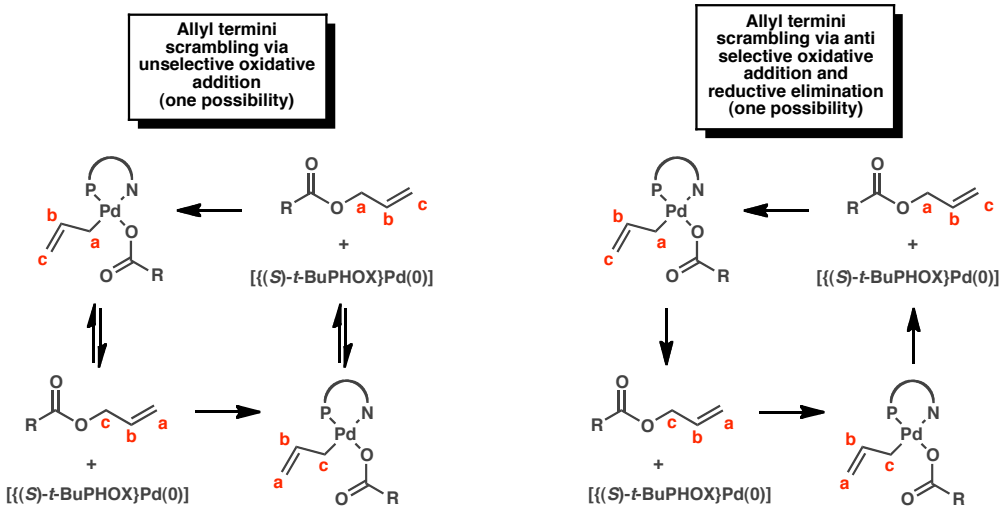

3.6 Effects on the Decarboxylative Allylic Alkylation of Ketone Enolates

As carboxylate **31** represents the resting state of the catalyst for decarboxylative asymmetric allylic alkylation of the allyl β-keto ester substrates,[1] by definition, the catalyst spends most of its time as carboxylate **31**. The similar reaction behavior observed for allyl enol carbonate substrates has suggested that there is likely an enol carbonate intermediate (such as **30**) which fills the same roll as carboxylate **31** (Figure **30**).[1] Together the chemical behavior of carboxylate **31** and putative carbonate **30** are expected to have a significant impact on the behavior of the reaction as a whole due to their prominence in it. Indeed, it appears that much of the allyl scrambling and exchange behavior that has been observed for the allylic alkylation system can be attributed to **31** and **30**, respectively.

*Figure 3.16. Carbonate **30**, the Putative Allyl Enol Carbonate Derived Analogue to Carboxylate **31***

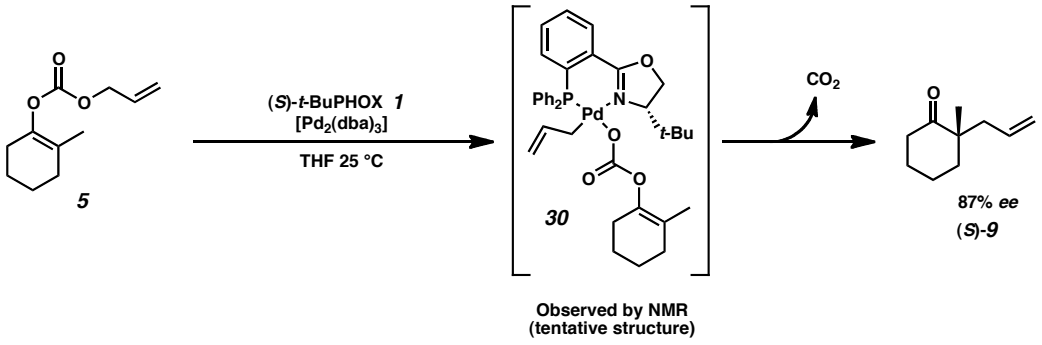

Via a crossover experiment from a previous mechanistic investigation, the decarboxylative asymmetric allylic alkylation was shown to give a product distribution consistent with complete crossover in conjunction with complete allyl termini scrambling (Scheme 3.8 on page 153).[2,27] Based on our originally proposed mechanism from a previous DFT study,[2,3] there was no satisfying explanation for the net transfer of enolate fragments that would be necessary to produce crossover. Rationalization of crossover

was especially challenging given the inability of earlier mechanistic studies to demonstrate the presence of a free enolate in solution at any point of the reaction.[2] Similarly, of the intermediates ascribed to the mechanism from the previous DFT study,[2,3] only π-allyl cation **25** was considered a possible candidate for producing the allyl termini scrambling seen in the crossover experiment.

Scheme 3.8. Crossover Experiment Shows Complete Crossover and Allyl Termini Scrambling[27]

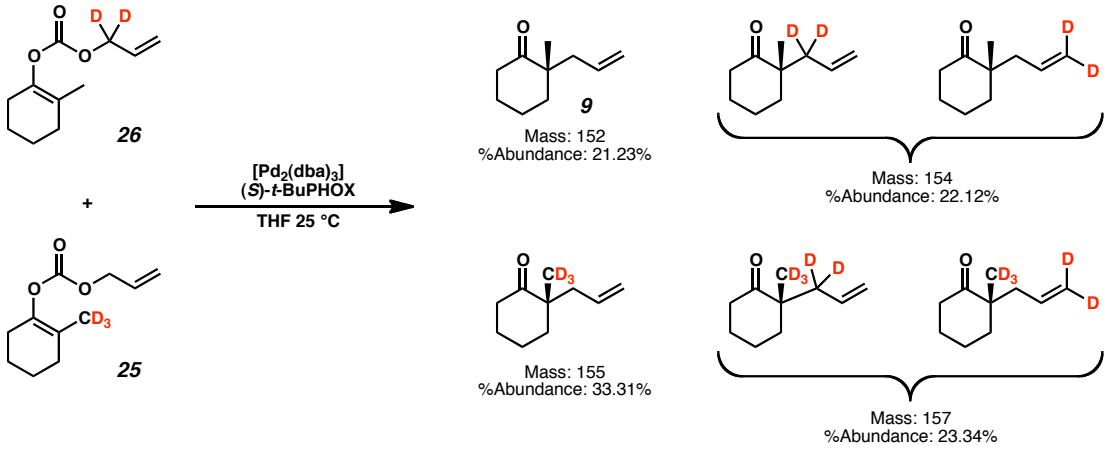

To the contrary, it appears that π-allyl cation **25** has little dynamic behavior in THF solution and is unable to exchange any of the termini for the allyl ligand. Instead, both allyl termini scrambling and crossover are caused by the long-lived intermediates **31** and **30**. Carboxylate **31** demonstrates extremely rapid exchange of carboxylate fragments and allyl termini scrambling even 55 °C below the temperature specified in the standard allylic alkylation conditions. Thus, the solution behavior of carboxylate **31**, and by analogy carbonate **30**, can fully account for the crossover and allyl termini scrambling observed in the products of the decarboxylative asymmetric allylic alkylation.

Specifically, it appears that allyl termini scrambling is the result of some combination of non-selective oxidative addition or reductive elimination of an allylic alkylation substrate to and from species such as **31** and **30**. If so, improving the

selectivity of these elementary steps should yield allylic alkylation conditions that have good regiocontrol over the allyl terminus where allylic alkylation occurs. Altogether a complete picture of the solution chemical behavior for complexes **31**, **32**, and **25** emerges (Figure 3.17 on page 154).

*Figure 3.17. Complete Solution Behavior for Complexes **31**, **32**, and **25***

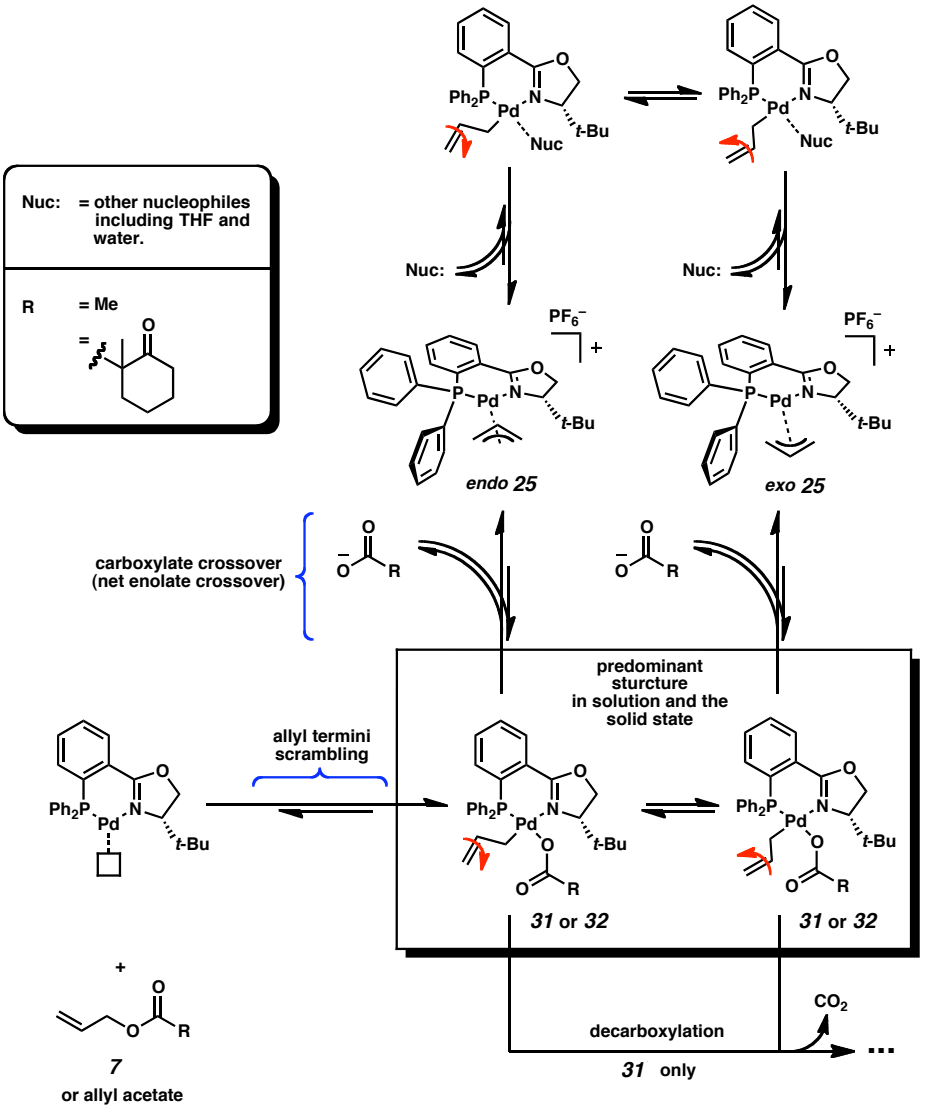

3.7 Experimental Procedures

3.7.1 Materials and Methods

Complexes **31**, **32**, and **25** • PF_6^- • 1/2EtOH have been previously characterized and were prepared as previously reported.[1] After synthesis, **25** • PF_6^- • 1/2EtOH was dried in vacuo for 24nh before being cycled into a nitrogen glovebox and recrystallized from anhydrous THF and then stored in the glove box. The NMR solvents $CDCl_3$ and $THF_{d\text{-}8}$ were purchased from Cambridge Isotope Laboratories and used as received. $THF_{d\text{-}8}$ was purchased as 1 or 0.75 mL ampoules, which were only used in a nitrogen glove box to exclude water. ^1H NMR spectra are reported relative to residual $CHCl_3$ (δ 7.26)[28] or to the downfield proton in residual $THF_{d\text{-}7}$ (δ 3.58).[28] ^{13}C NMR spectra are reported relative to $CDCl_3$ (δ 77.16)[28] or to the downfield carbon in $THF_{d\text{-}8}$ (δ 67.21).[28] ^{31}P NMR spectra are reported relative to H_3PO_4 (δ 0.00) as an external standard consisting of 85% neat phosphoric acid. All filtrations performed in a glove box or otherwise associated directly or indirectly with inorganic or organometallic complexes were performed exclusively with scintillated glass Buchner funnels or using 2.4 mm GF/A Whatman glass microfiber filter paper.

3.7.2 Measuring the Kinetics and Activation Parameters for Exo/Endo *Allyl Isomerization in π-Allyl Cation **25** via Saturation Transfer*

3.7.2.1 Kinetics Measurements Via Saturation Transfer for π-Allyl Cation 25

Sample Preparation and Setup: In a nitrogen glove box, 10 mg of the half ethanol adduct of π-Allyl Cation **25** PF_6^- salt (14 μmol, 1 equiv) was weighed into a 1 dram vial. A fresh ampule of $THF_{d\text{-}8}$ was opened and added to the vial. The contents

were mixed manually by pipette until all the material had dissolved. This solution was filtered into an NMR tube, which was sealed with an appropriately fitted septum, and the tube was removed from the glove box. For the run with 4.4 equiv water, the intended amount of distilled water (1.1 μL, 1.1 mg, 63 μmol, 4.4 equiv) was added to the solution via a microliter syringe outside the glove box, and the tube was inverted once to mix the contents.[29] An initial ^{1}H NMR spectrum was obtained at 25 °C, and the actual water content was measured by integrating the water resonance against resonances of the π-Allyl Cation **25**.[30] The solution was cooled in the NMR down to the highest temperature where the *exo* and *endo t*-Bu resonances did not show an appreciable amount of overlap due to the beginnings of coalescence (qualitatively determined to be 10 °C with 3.04 mol% water, and 5 °C for 4.4 equiv water). Then measurements (see procedure below) were taken every 5 °C down to –25 °C or –30 °C just into the temperature range that coincides with an apparent change in rate determining step (*vide infra*, see Section 3.7.2.2 on page 159)

Measurement Procedure: At each temperature, a T_1 measurement of both the *exo* and *endo t*-Bu group resonances was acquired using a standard inversion recovery method. Two arrays of presaturation experiments were taken which arrayed varying saturation delay times starting at zero. The d1 for all the presaturation experiments was set to at least five times the measurement for the largest T_1 found between the *t*-Bu resonances at that temperature. The two arrays of presaturation experiments were used to obtain the peak height (h) of the *exo t*-Bu resonance when presaturating the *endo t*-Bu resonance, and vice versa, at both T_0 [$h(T_0)$ = peak high at zero saturation delay] and T_∞

[$h(T_\infty)$ = the height of the asymptote approached by the diminishing resonance across the array of increasing saturation delay times]. The rate constant k was calculated by:

$$k = \frac{h(T_0) - h(T_\infty)}{T_1 \bullet h(T_\infty)}.$$

Raw Data and Calculations for 3.04 mol% Water:

T_1 Measurements for 3.04 mol% Water

temp (°C)	*endo* T_1 (s)	*endo* T_1 error	*exo* T_1 (s)	*exo* T_1 error
-25	0.2418	0.0007074	0.2463	0.0007295
-20	0.2524	0.0005425	0.2562	0.0006287
-15	0.2598	0.001489	0.2662	0.001066
-10	0.2773	0.0006935	0.2815	0.0008757
-5	0.292	0.001097	0.2965	0.001009
5	0.3289	0.0009827	0.3326	0.0007701
10	0.3461	0.001694	0.35	0.001214

Presaturation Measurements for 3.04 mol% Water

temp (°C)	*endo* $h(T_0)$	*endo* $h(T_\infty)$	*exo* $h(T_0)$	*exo* $h(T_\infty)$
-25	360.721	272.416	634.514	493.685
-20	379.217	270.551	678.541	514.621
-15	381.904	246.14	710.52	517.925
-10	340.202	189.119	650.277	431.42
-5	328.49	153.946	649.126	381.766
5	253.17	73.7155	546.659	219.197
10	223.261	49.995	505.922	165.137

Calculated Rates for 3.04 mol% Water

temp (°C)	$k_{exo \rightarrow endo}$ (s^{-1})	$k_{endo \rightarrow exo}$ (s^{-1})
-25	1.158184509	1.340591269
-20	1.243269603	1.591311447
-15	1.396915326	2.123064957
-10	1.802111957	2.880915814
-5	2.361970598	3.882877273
5	4.491630882	7.40170316
10	5.896143375	10.01348329

Raw Data and Calculations for 4.4 Equiv Water:

T_1 Measurements for 4.4 Equiv Water

temp (°C)	*endo* T_1 (s)	*endo* T_1 error	*exo* T_1 (s)	*exo* T_1 error
-30	-30	0.2254	0.0006561	0.2286
-25	-25	0.2361	0.0004719	0.2397

-20	-20	0.2502	0.0009163	0.2547
-15	-15	0.259	0.001098	0.2616
-10	-10	0.278	0.001051	0.2789
-5	-5	0.293	0.0007455	0.2947
0	0	0.311	0.001166	0.3117
5	0.3331	0.001309	0.3316	0.001599

Presaturation Measurements for 4.4 Equiv Water

temp (°C)	*endo* $h(T_0)$	*endo* $h(T_\infty)$	*exo* $h(T_0)$	*exo* $h(T_\infty)$
-30	181.613	119.566	310.764	222.038
-25	192.922	115.159	349.838	235.673
-20	203.288	103.99	386.761	244.723
-15	199.622	84.6114	397.716	220.118
-10	155.716	51.3619	333.117	155.896
-5	142.439	36.5186	323.736	119.183
0	124.587	23.9298	294.784	86.6597
5	105.811	16.8408	261.461	62.6516

Calculated Rates for 4.4 Equiv Water

temp (°C)	$k_{exo \rightarrow endo}$ (s^{-1})	$k_{endo \rightarrow exo}$ (s^{-1})
-30	1.158184509	1.340591269
-25	1.243269603	1.591311447
-20	1.396915326	2.123064957
-15	1.802111957	2.880915814
-10	2.361970598	3.882877273
-5	4.491630882	7.40170316
0	5.896143375	10.01348329
5	1.158184509	1.340591269

3.7.2.2 Eyring Plot and Activation Parameters for π-Allyl Cation 25

All Data Plotted for *Exo* to *Endo*

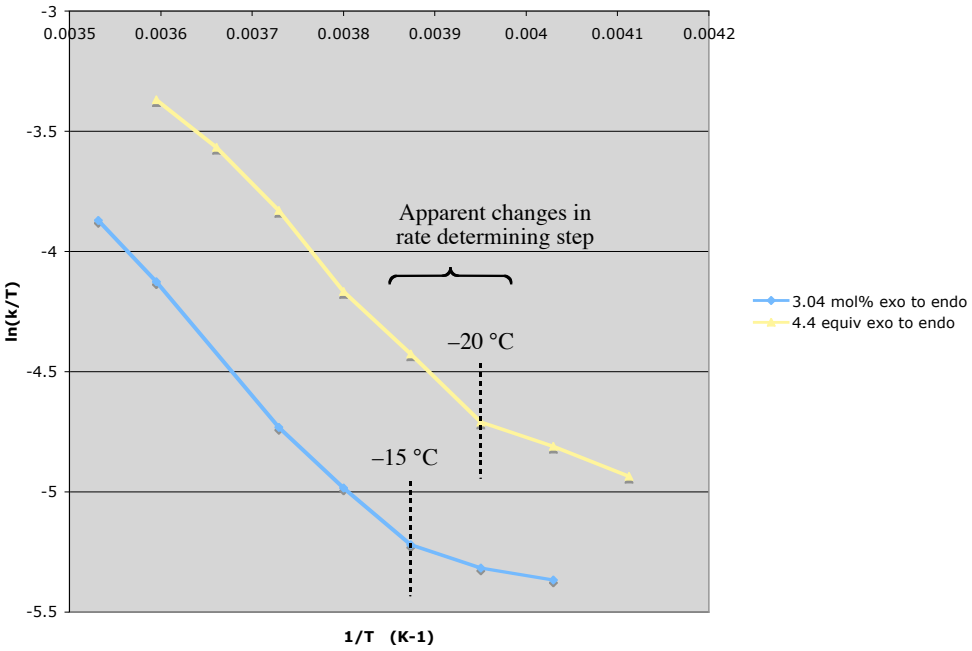

All Data Plotted for *Endo* to *Exo*

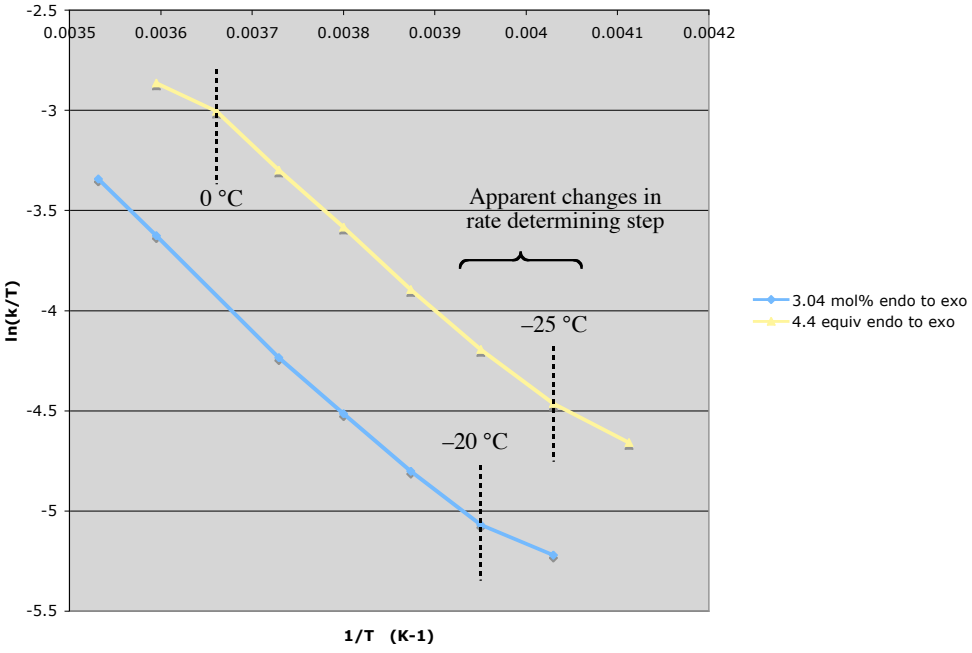

Best Single Rate Data Plotted for *Exo* to *Endo*

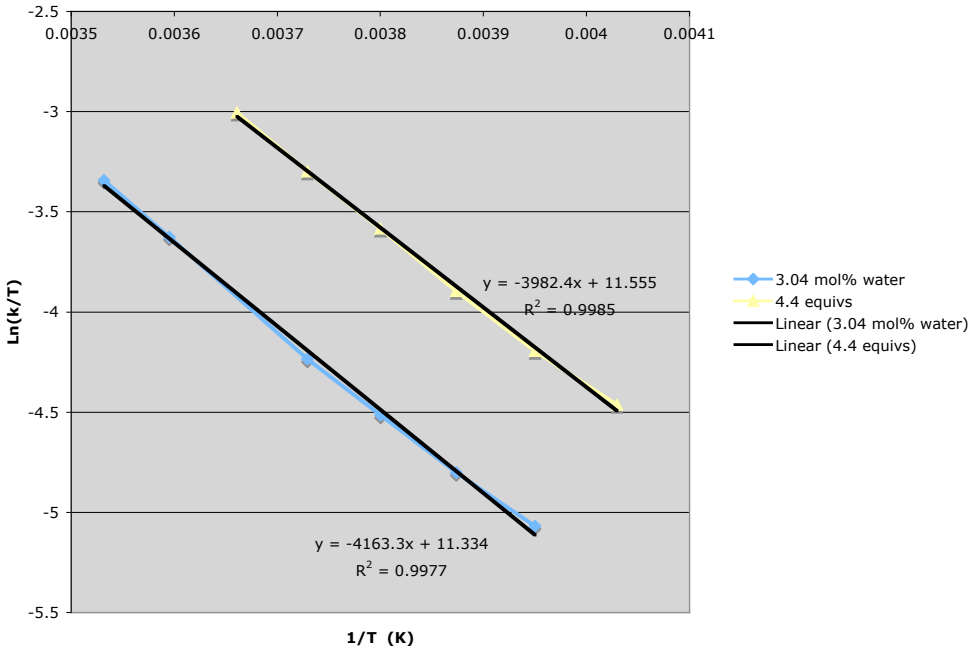

Best Single Rate Data Plotted for *Endo* to *Exo*

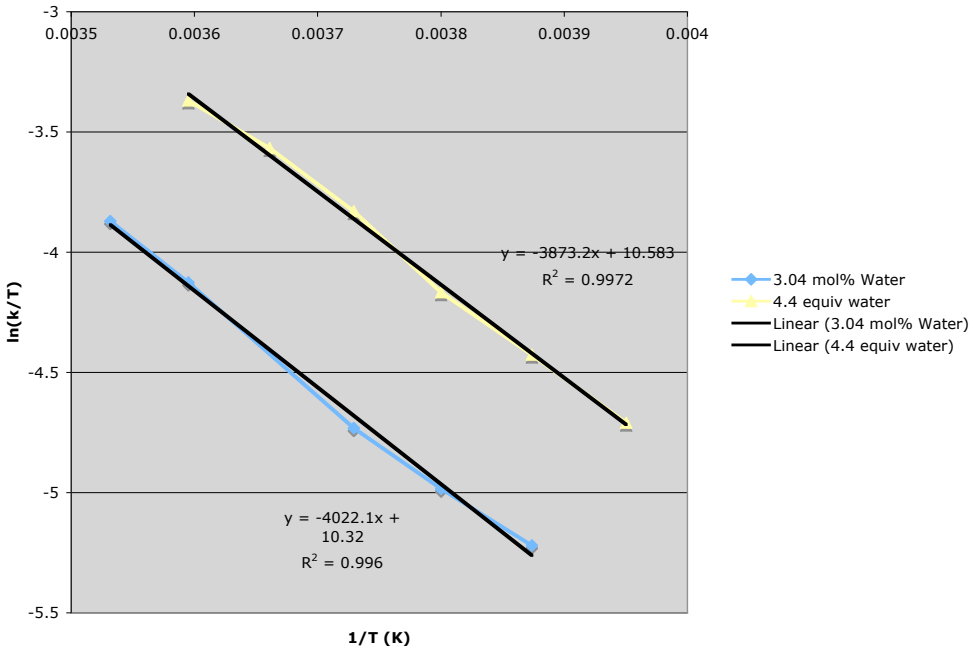

Raw Eyring Plot Parameters

Added Water	Slope *exo→endo* (K)	Slope *endo→exo* (K)	Intercept *exo→endo*	Intercept *endo→exo*
3.04 mol%	-4022.1	-4163.3	10.32	11.334
4.4 equiv	-3873.2	-3982.4	10.58	11.555

$\Delta S^{\ddagger}$ (J mol^{-1} K^{-1}) = R • [Intercept – ln(k_b/h)]

$\Delta H^{\ddagger}$ (J mol^{-1}) = –R • slope

Activation Parameters

Added Water	$\Delta H^{\ddagger}$ (kcal/mol) *exo→endo*	$\Delta H^{\ddagger}$ (kcal/mol) *endo→exo*	$\Delta S^{\ddagger}$ (kcal/mol•K) *exo→endo*	$\Delta S^{\ddagger}$ (kcal/mol•K) *endo→exo*
3.04 mol%	8.0	8.3	–27	–25
4.4 equiv	7.7	7.9	–26	–24

(1) See Chapter 2, or Sherden, N. H.; Behenna, D. C. Virgil, S. C. Stoltz, B. M. *Angew. Chem., Int. Ed.* **2009**, *48*, 6840–6843.

(2) See Chapter 1.

(3) (a) Keith, J. A. *Computational Insight into Homogeneous Organopalladium Catalysis*, Ph.D. Thesis, California Institute of Technology, Pasadena, CA, **2008**. (b) Keith, J. A.; Behenna, D. C.; Mohr, J. T.; Ma, S.; Marinescu, S. C. Oxgaard, J.; Stoltz, B. M. Goddard, W. A., III. *J. Am. Chem. Soc.* **2007**, *129*, 11876–11877.

(4) (a) Grennber, H.; Langer, V.; Bäckvall, J.-E. *J. Chem. Soc. Chem. Commun.* **1991**, 1190–1192. (b) Bäckvall, J.-E.; Hopkins, R. B.; Grennberg, H.; Mader, M. M.; Awasthi, A. K. *J. Am. Chem. Soc.* **1990**, *112*, 5160–5166.

(5) (a) Moiseev, I. I.; Vargaftik, M. N. *Coord. Chem. Rev.* **2004**, *248*, 2381–2391. (b) Hansson, S.; Heumann, A.; Rein, T.; Åkermark, B. *J. Org. Chem.* **1990**, *55*, 975–984. (c) Byström, S. E.; Larsson, E. M.; Åkermark, B. *J. Org. Chem.* **1990**, *55*, 5674–5675. (d) Åkermark, B.; Hansson, S.; Rein, T.; Vågberg, J.; Heumann, A.; Bäckvall, J.-E. *J. Organomet. Chem.* **1989**, *369*, 433–444.

(6) Bäckvall, J.-E.; Byström, S. E.; Nordberg, R. E. *J. Org. Chem.* **1984**, *49*, 4619–4631.

(7) For the 2D NMR spectra see the **XX** section of the experimentals section.

(8) For the synthesis and discussion of some of the first and most highly related palladium η^1-allyls, see: (a) Zhang, J.; Braunstein, P.; Welter, R. *Inorg. Chem.* **2004**, *43*, 4172–4177. (b) Braunstein, P.; Zhang, J.; Welter, R. *Dalton Trans.* **2003**, 507–509. (c) Kollmar, M.; Helmchen, G. *Organometallic*, **2002**, *21*, 4771–4775. (d) Braunstein, P.; Naud, F.; Dedieu, A.; Rohmer, M.-M.; DeCian, A.; Rettig, S. J. *Organometallics* **2001**, *20*, 2966–2981.

(9) For a more recent publication of a highly related palladium η^1-allyl complex, see: Canovese, L.; Visentin, F.; Santo, C.; Chessa, G.; Bertolasi, V. *Organometallics* **2010**, *29*, 3027–3038.

(10) For the ^{1}H and ^{13}C NMR chemical shifts of simple organic compounds, such as free propene and allyl acetate, dissolved in various common NMR solvents, including $THF_{d\text{-}8}$, see: Fulmer, G. R.; Miller, A. J. M.; Sherden, N. H.; Gottlieb, H. E.; Nudelman, A.; Stoltz, B. M.; Bercaw, J. E.; Goldberg, K. I. *Organometallics* **2010**, *29*, 2176–2179.

(11) The EXSY NMR spectra refers to the cross peaks that are in phase with the diagonal of either a ROESY or NOESY NMR spectra. While the cross peaks of phase opposite to the diagonal in these spectra represent through-space contacts, the in-phase cross peaks represent chemical exchange and are referred to as the EXSY spectra. The EXSY spectra for **32** and **25** is interpreted from NOESY spectra while the EXSY spectra for **31** is interpreted from the ROESY spectra of the complex. The latter is necessary as the mass of complex **31** in conjunction with the reduced temperatures necessary to preserve **31** in solution long enough to take 2D NMR (–20 °C) makes for a more viscous solution and causes the product of the rotational correlation time and the Larmor frequency to approach the NOESY null. NOESY spectra taken on samples approaching the null can cause EXSY and nOe cross peaks to become indistinguishable from one another or even disappear into the background noise.

(12) In the exchange diagrams in this chapter (Figure 3.4 and Figure 3.5), the diagonal is grayed as a reference point and to signify that there can be no meaningful data for these spaces. A square containing an "s" signifies a strong EXSY cross-peak, i.e. the two protons interconvert rapidly and the EXSY cross-peak is not diminished by an overlapping NOESY or ROESY signal. A square containing a "w" signifies a weak EXSY cross-peak. A weak EXSY cross-peak can signify a slower exchange of protons than a more strongly exchanging cross peak, or a strong EXSY cross-peak that is diminished in intensity due to an overlap with a NOESY or ROESY cross-peak. The later is expected to be the case for $1_\alpha \leftrightarrow 1_\beta$ as depicted in Figure 3.4 for complex **32**, as complex **31** shows a clear ROESY cross-peak between the equivalent 1_α and 1_β protons. A square containing an "i" means an implied exchange. In such cases there is reason to expect an EXSY cross-peak between the two indicated protons, but instead a weak NOESY or ROESY signal is present and is presumed to be eclipsing the expected EXSY cross-peak (see endnote 13). An empty square means these protons do not show any signs of exchange.

(13) Both sets of terminal protons, $1_\alpha/1_\beta$ and $3_\alpha/3_\beta$, for complexes **31** and **32** have strong nOe interactions between one another (i.e., $1_\alpha \leftrightarrow 1_\beta$ and $3_\alpha \leftrightarrow 3_\beta$) that create nOe cross-peaks directly on top of and of the opposite phase of the EXSY cross-peaks generated by chemical exchange. This phenomena is responsible for

the weak EXSY signal between 1_α and 1_β shown in Figure 3.4 for complex **32**. This is borne out by the rOe instead of EXSY cross-peak between 1_α and 1_β demonstrated in the related complex **31** at a lower temperature (–20°C instead of 0°C). At lower temperatures chemical exchange would be expected to be slower, and thus EXSY cross-peaks would be weaker relative to eclipsing rOe or nOe cross-peaks. Thus, the reduced temperature explains the $1_\alpha \leftrightarrow 1_\beta$ exchange being completely obscured by a rOe cross-peak for complex **31** while only being weakened for complex **32** at a higher temperature. As a result it is assumed that both sets of protons, $1_\alpha/1_\beta$ and $3_\alpha/3_\beta$, for both **31** and **32** are in direct exchange (i.e., $1_\alpha \leftrightarrow 1_\beta$ and $3_\alpha \leftrightarrow 3_\beta$) even though most of these implied exchange cross-peaks cannot be directly observed in the EXSY spectrum. Even in the unlikely event where these protons do not undergo direct exchange, they can still exchange indirectly via EXSY observable paths such as: $1_\alpha \rightarrow 1_\beta$ via $1_\alpha \rightarrow 3_\beta$ then $3_\beta \rightarrow 1_\beta$. Given how rapid the direct exchange paths appear to be, even such an indirect exchange path should result in an EXSY cross-peak between the two protons (i.e., $1_\alpha \rightarrow 1_\beta$) under the given conditions. This suggests yet again that the EXSY cross-peaks for $1_\alpha \leftrightarrow 1_\beta$ and $3_\alpha \leftrightarrow 3_\beta$ exist, but are obscured by eclipsing NOESY or ROESY cross-peaks. As such, the exchange paths $1_\alpha \leftrightarrow 1_\beta$ and $3_\alpha \leftrightarrow 3_\beta$ are implicit.

(14) There is little discussion in the literature about allyl termini scrambling for palladium η^1-allyl species. It is occasionally noted, however, that the allyl ligands found in isolable palladium η^1-allyl species are not fluxional, and do not seem to have any exchange paths at all let alone those that would allow for allyl termini scrambling. Also, published studies of the dynamic behavior of fluxional palladium η^1-allyl species rarely results in a report of allyl termini exchange. Instead the reported fluxional behaviors are typically the result of other ligands on the complex changing conformation or binding. For select examples of fluxional palladium η^1-allyl species see references 8a,b,d.

(15) For some select examples and relavent discussion see: (a) Vázquez, J.; Goldfuss, B.; Helmchen, G.; *J. Organomet. Chem.* **2002**, *641*, 67–70. (b) Kollmar, M.; Steinhagen, H.; Janssen, J. P.; Goldfuss, B.; Malinovskaya, S. A.; Vázquez, Rominger, F.; Helmchen, G. *Chem.—Eur. J.* **2002**, *8*, 3103–3114. (c) Kollmar, M.; Goldfuss, B.; Reggelin, M.; Rominger, F.; Helmchen, G. *Chem.—Eur. J.* **2001**, *7*, 4913–4927. Also see reference 18b.

(16) An extremely unlikely and unprecedented fourth mechanism could also theoretically explain this diastereotopic chemical exchange cross-peak: the allyl ligand 1_α protons could be physically transferred between the two diastereomers of **31**. Beyond being an unlikely proposition in its own right, such a process would result in deuteria migrating from the di-deuterated allyl ligand to other allyl ligands in the allyl enol carbonate cross-over experiment (see **XX**). Thus, if this hypothetical allyl ligand proton exchange pathway were operative, the cross-over

experiment should have also produced ketone **9** with mono-, tri-, and tetra-deuterated allyl ligands. Such products were not observed.

(17) The stereochemical enrichment found when synthesizing carboxylate **31** is expected to be a result of a kinetic resolution occurring somewhere in the course of the decarboxylative asymmetric allylic alkylation. Current results suggest that decarboxylation may actually be slightly faster for the (*S*,*S*)-diastereomer relative to the (*R*,*S*)-diastereomer of carboxylate **31**, thus resulting in a kinetic resolution that can stereochemically enrich this intermediate. Alternately it is possible that one diastereomer of **31** is more soluble then the other, and thus purification of carboxylate **31**, which is done via recrystalization, results in diastereomeric enrichment of **31** even though both diastereomers co-crystallize. However, the stereochemical enrichment of the quaternary stereocenter in **31** being the result of stereoselective deallylation of allyl β-ketoester **7** has been disproved.

(18) (a) Johns, A. M.; Utsunomiya, M.; Incarvito, C. D.; Hartwig, J. F. *J Am. Chem. Soc*. **2006**, *128*, 1828–1839. (b) Hansson, S.; Norrby, P.-O.; Sjögren, M. P. T.; Åkermark, B.; Cucciolito, M. E.; Giordano, F.; Vitagliano, A. *Organometallics* **1993**, *12*, 4940–4948. (c) Åkermark, B.; Åkermark, G.; Hegedus, L. S.; Zettergerg, K. *J. Am. Chem. Soc*., **1981**, *103*, 3037–3040.

(19) In every literature report, when a ligand *cis* to an η^1-allyl ligand on palladium is removed from the complex, the η^1-allyl ligand isomerizes η^3 and fills the newly vacated coordination site extremely rapidly. This results in the generation of the corresponding palladium π-allyl species, typically a π-allyl cation. For select examples, see reference 8. By analogy, a palladium η^1-allyl complex with a *cis* labile ligand, such as carboxylate, should also result in the corresponding π-allyl species whenever the labile *cis* ligand disassociates from the palladium center.

(20) The EXSY spectra for palladium π-allyl cation **25** in $THF_{d\text{-}8}$ shows an identical means of η^3-η^1-η^3 (or π-σ-π) conversion between its *exo* and *endo* isomers as is shown in the EXSY spectra published for the highly related unsubstituted palladium π-allyl cation of the *i*-Pr PHOX ligand in $CDCl_3$, published by Helmchen. See: Sprinz, J.; Kiefer, M.; Helmchen, G. *Tetrahedron Lett*., **1994**, *35*, 1523–1526.

(21) (a) Pregosin, P. S.; Salzmann, R.; Togni, A. *Organometallics* **1995**, *14*, 842–847. (b) Abbenhuis, H. C. L.; Burckhardt, U.; Gramlich, V.; Köllner, C.; Pregosin, P. S.; Salzmann, R.; Togni, A. *Organometallics* **1995**, *14*, 759–766. (c) Breutel, C.; Pregosin, P. S.; Salzmann, R.; Togni, A. *J. Am. Chem. Soc*. **1994**, *116*, 4067–4068.

(22) Different nucleophiles, especially those of different strengths, may have different preferences for how they bind to complex **25**. While carboxylate nucleophiles have demonstrated a distinct preference for binding in the square plane via

carboxylates **31** and **32**, it is entirely possible that weaker nucleophiles, such as THF or water, might only associate at the apical position of π-allyl cation **25**. Beyond their association with the metal center, nothing more can be said about where isomerization catalyzing nucleophiles might prefer to bind to π-allyl cation **25** from the current data.

(23) For an NMR study of the solution behavior for palladium π-allyl complexes possessing a larger set of allyl isomerization modes, including apparent allyl rotation, and an in-depth discussion thereof, see reference 18b.

(24) (a) Evans, L.; A.; Fey, N.; Harvey, J. N.; Hose, D.; Lloyd-Jones, G. C.; Murray, P.; Orpen, A. G.; Osborne, R.; Owen-Smith, G. J. J.; Purdie, M. *J. Am. Chem. Soc*. **2008**, *130*, 14471–14473. (b) Amatore, C.; Bahsoun, A. A.; Jutand, A.; Mensah, L.; Meyer, G.; Ricard, L. *Organometallics* **2005**, *24*, 1569–1577. (c) Amatore, C.; Gamez, S.; Jutand, A. *Chem.—Eur. J*. **2001**, *7*, 1273–1280.

(25) For a thorough mechanistic discussion about the allyl terminus regioselectivity of outer-sphere allylic alkylation on palladium using the PHOX ligand architecture, see: (a) Helmchen, G.; Steinhagen, H.; Reggelin, M.; Kudis, S. In *Selective Reactions of Metal-Activated Molecules*, (Eds. Werner, H.; Schreier, P.), Vieweg Verlag, Wiesbaden, **1998**, 205–215. (b) Helmchen, G. *J. Organomet. Chem*. **1999**, *576*, 203–214. (c) Steinhagen, H.; Reggelin, M.; Helmchen, G.; *Angew. Chem., Int. Ed*. **1997**, 2108–2110. (d) Helmchen, G.; Kudis, S.; Sennhenn, P. Steinhagen, H. *Pure Appl. Chem*. **1997**, *69*, 513–518. (e) Sprintz, J.; Kiefer, M.; Helmchen, G.; Reggelin, M.; Huttner, G.; Walter, O.; Zsolnal, L. *Tetrahedron Lett*. **1994**, *35*, 1523–1526.

(26) In turn, this implies that system redesigns that influence allyl termini selectivity of oxidative addition towards the same preference seen in reductive elimination might allow for kinetic instead of thermodynamic regiocontrol on the allyl fragment of terminally substituted allylic alkylation products. Among other possibilities such kinetic regiocontrol could allow for palladium-catalyzed allylic alkylation processes selective for the branched allyl product, which is in stark contrast to the high preference for linear allylic alkylation products generally exhibited by palladium species (for a very brief discussion and some examples of the allyl termini selectivity preference found in palladium-catalyzed allylic alkylation see Chapter 1).

(27) Mohr, J. T.; Behenna, D. C.; Harned, A. M.; Stoltz, B. M. *Angew. Chem., Int. Ed*. **2005**, *44*, 6924–6927.

(28) Fulmer, G. R.; Miller, A. J. M.; Sherden, N. H.; Gottlieb, H. E.; Nudelman, A.; Stoltz, B. M.; Bercaw, J. E.; Goldberg, K. I. *Organometallics* **2010**, *29*, 2176–2179.

(29) For the run with 3.04 mol% water, no water was manually added. It is likely the 3.04 mol% water came from π-allyl cation **25**, which was prepared on the bench top and recrystallized from ethanol as previously published,[1] before being subjected to extended drying in vacuo giving ample opportunity for the sample of **25** to pick up a small amount of moisture. Alternatively, as THF solutions of **25** PF_6^- are fairly hygroscopic, the 3.04 mol% water may have leaked into the NMR tube after the sample was prepared.

(30) When integrating against π-Allyl Cation **25**, the resonances from both the *endo* and *exo* isomers were integrated and the value was added together. Water was integrated against the smaller resonances of π-Allyl Cation **25** such as the oxazoline or π-Allyl proton resonances. For each run, a few such resonances in π-Allyl Cation **25** were selected at random and the concentration of water was reported as an average of integrating against these resonances. The chemical shift of water in $THF_{d\text{-}8}$ is δ = 2.46 ppm (see reference 28).